

Flux-Driven Circular Current in a Non-Hermitian Dimerized Aharonov-Bohm Ring: Impact of Physical Gain and Loss

Souvik Roy^{1,*} and Santanu K. Maiti^{1,†}

¹*Physics and Applied Mathematics Unit, Indian Statistical Institute,
203 Barrackpore Trunk Road, Kolkata-700 108, India*

In the present work, we explore magnetic response of a dimerized ring subjected to Aharonov-Bohm (AB) flux and environmental interactions. Specifically, we introduce an imaginary site potential on the odd lattice sites to represent physical gain and loss, while the even lattice sites remain unperturbed. We investigate the induced current resulting from the AB flux in both real and imaginary eigenspaces, aiming to enhance this current significantly by adjusting the gain/loss parameter (d). Our analysis focuses on how exceptional points in the real and imaginary eigenenergy spaces contribute to notable increases in current at specific d values, and the emergence of purely real current when the imaginary current vanishes. We focus on how the converging and diverging nature of the energy spectrum leads to gradual increases and decreases in the current. Additionally, we study the interplay between the correlations of dimerized hopping integrals and the gain-loss parameter, which affects the current and highlights key features associated with these physical parameters. Furthermore, we consider how system size impacts our findings. These investigations may reveal unconventional characteristics in various loop configurations, potentially paving the way for new research directions.

I. INTRODUCTION

Recent studies have focused intensely on various non-Hermitian (NH) systems, particularly those that transform into parity-time (PT) symmetric configurations upon accounting for environmental interactions^{1–5}. Such systems have garnered significant attention across research domains. Non-Hermiticity in these contexts can arise from non-reciprocal hopping integrals or complex site potentials. Depending on the sign of the complex potential, these systems may exhibit either gain or loss, crucial for maintaining PT symmetry through balanced distributions. Under specific parameter regimes, PT symmetric NH systems^{6–10} can feature a real energy spectrum and display intriguing characteristics. Notably, exceptional points and non-orthogonal eigenmodes have been identified in optical NH systems, where proximity to exceptional points has been associated with phenomena like heightened sensing, sensitivity, diffusive coherent transport, topological states, and the skin effect as documented in literature. Such NH and PT symmetric systems^{11–16} have also been extensively explored in electronics, sound propagation, electromagnetic wave propagation in media with complex refractive indices, and aspects of atomic and nuclear physics. Theoretical and experimental investigations abound, probing into the diverse physics inherent in these systems. In addition to these, localization phenomena in closed systems and quantum transport^{17–23} in open quantum systems have been investigated in various NH systems. In the analysis of quantum transport, exceptional points play a crucial role in probing the behavior of transmission function. The influence of physical gain and loss^{24–53} is also significant in the context of extended-to-localized phase transitions^{54–67}. Exceptional points amplify the generation of circular currents and consequently induce a magnetic field in open quantum systems. Similarly, the behavior of circular currents in dimerized closed-loop geometries under AB flux can be examined, where odd lattice sites experience phys-

ical gain and loss, while even lattice sites remain perfect. To the best of our knowledge, such an investigation has

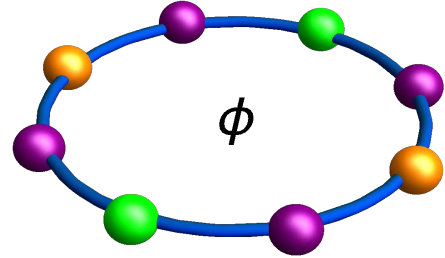


FIG. 1: (Color online). This diagram illustrates a one-dimensional ring system subjected to environmental interactions and threaded by an AB flux denoted by ϕ . In this schematic, the purple spheres represent the unperturbed lattice sites, while the orange and green spheres symbolize the presence of gain and loss respectively.

not been documented in the existing literature. Exploring the behavior of circular currents under AB flux in such NH systems represents a significant aspect of the mesoscopic era that we aim to explore in our current study.

According to Büttiker, Imry, and Landauer^{67–70}, if the current is originated in a ring in presence of AB flux, it will remain in the ring even after removal of flux^{71–75,77,78}. The behavior of current in disordered systems has been well studied in the literature^{79–91}. In general the current gets reduced with disorder strength^{92–100}. But upon some specific arrangement between the site energies and hopping dimerization the current can also be increased with disorder strength. The enhancement of current due to the interplay between site

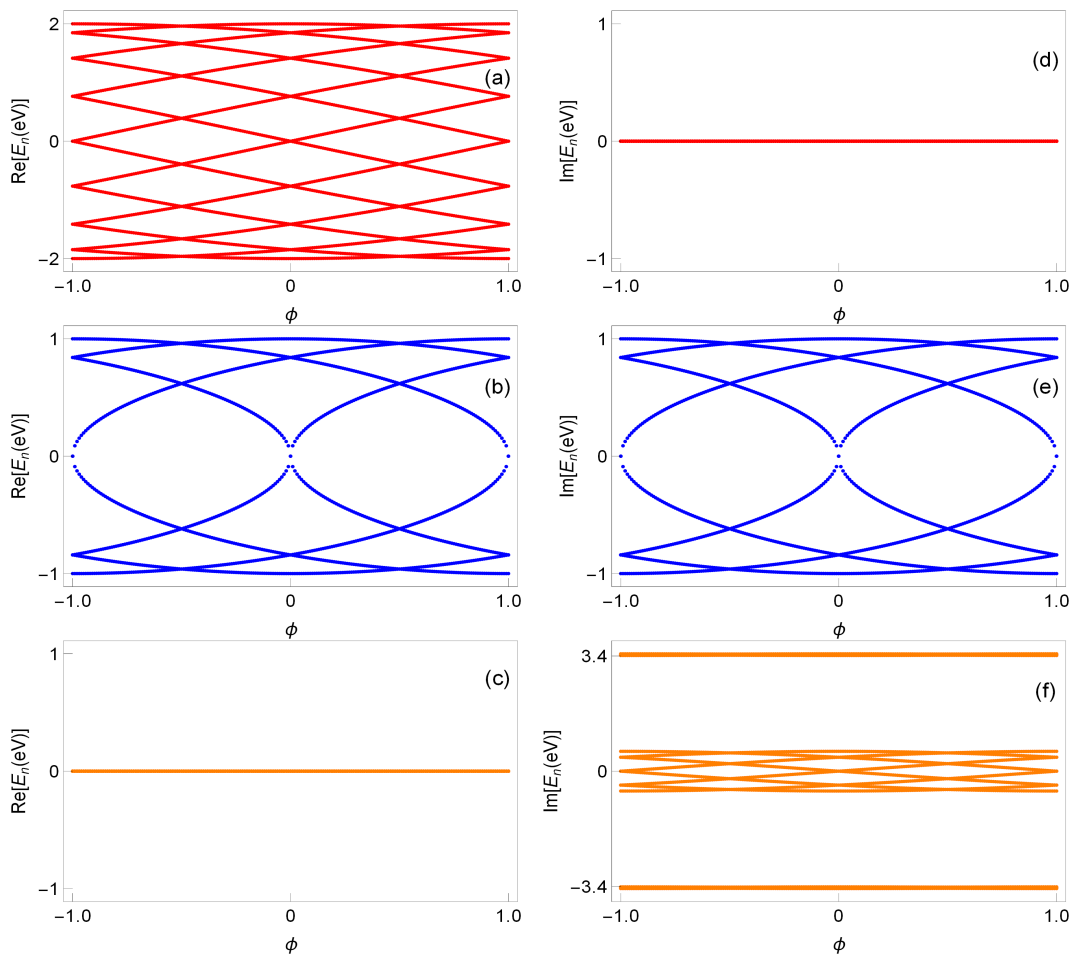


FIG. 2: (Color online). The figure presents a comparative analysis of the real and imaginary band spectra for a one-dimensional ring consisting of $N = 16$ sites, where the hopping integrals are equal ($t_1 = t_2$), under the influence of an applied AB flux. In the left column, the real part of the band spectrum is plotted, while the right column illustrates the corresponding imaginary band spectrum. The distinct colors are used to differentiate the values of the NH gain and loss parameter, d : the red curve corresponds to $d = 0$, the blue curve represents $d = 2$, and the orange curve illustrates the behavior at $d = 4$.

energies and hopping dimerization has been explored in previous studies^{101,102}. However, *the modulation of current in the presence of NH effects, particularly its dependence on the correlation between hopping integrals has received far less attention. Furthermore, this model offers a unique capability to sustain a purely real current up to a certain threshold of the NH parameter, despite the system being NH in nature. This distinct feature emphasizes the novel behavior introduced by the NH factor.* Hence, to explore different important characteristics of current in presence of environmental interaction, we take a ring and incorporates physical gain and loss alternatively only at the odd sites of the sample where the even lattice sites are keep free.

In this study, we aim to investigate various significant aspects of NH systems, such as the influence of environmental interaction parameter d and hopping dimerization on the band spectrum, transitions between real and complex eigenvalues, exceptional points, circular currents, and to name a few. We organize the real and imaginary eigenvalues into their respective domains and compute the ground state energy and current by differ-

entiating the ground state energy with respect to flux. The present study include several important aspects that are as follows. (i) The real band spectrum dominates at low gain-loss values but decreases as the imaginary spectrum becomes more prominent with increasing gain-loss. (ii) Initially, real and imaginary spectra exhibit degeneracies, which break down as the gain-loss parameter grows, altering the eigenvalue structure and leading to new behavior. (iii) A switching pattern in real and imaginary bands is observed based on the relative strength of hopping integrals, signaling transitions between different regimes as system parameters change. (iv) Real and imaginary currents behave similarly under certain conditions but diverge as parameters shift, revealing a strong correlation with hopping integrals and the gain-loss parameter. (v) Exceptional points near the zero-energy axis increase system's sensitivity, with peaks in real and imaginary currents appearing near these points, and an inverse relationship between the two currents is observed. (vi) When the hopping integrals differ, the gap between peaks in real and imaginary currents widens, a trend consistent even in larger system sizes, and NH sys-

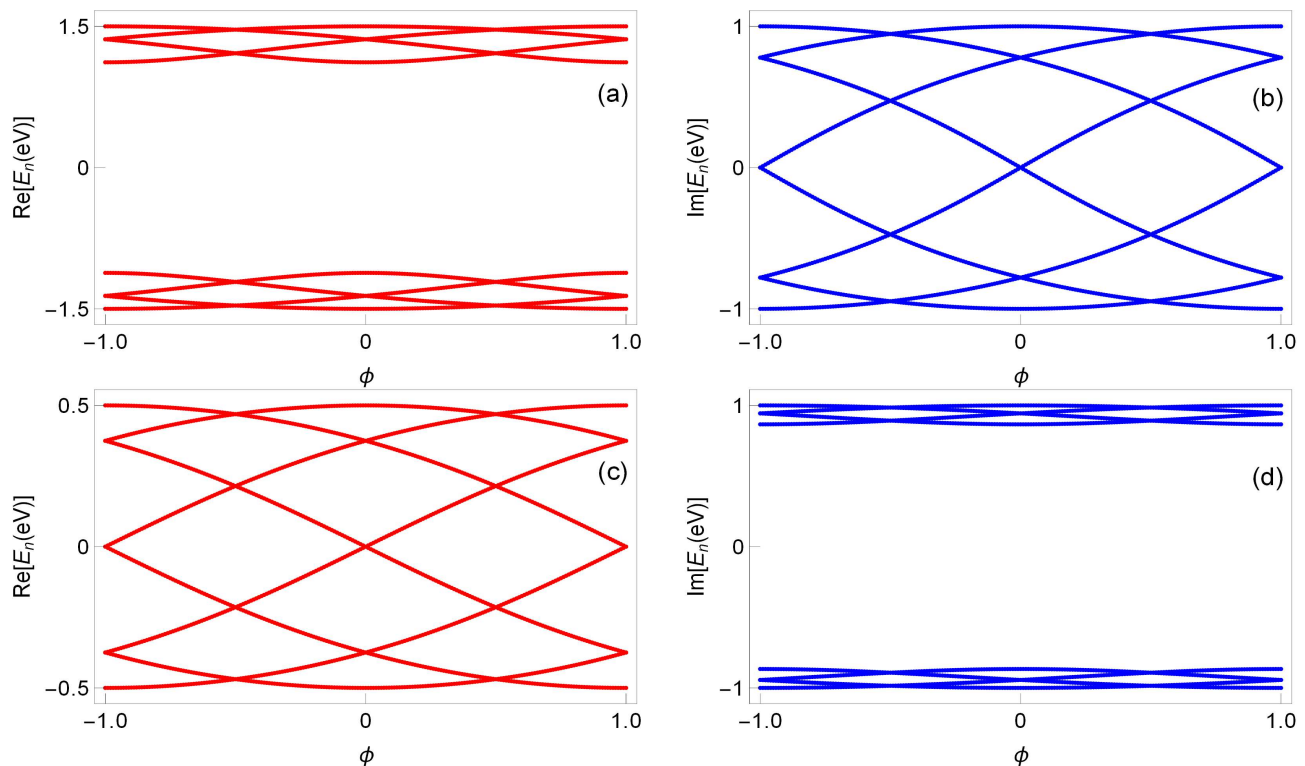


FIG. 3: (Color online). This figure illustrates the real and imaginary band spectra for a one-dimensional ring comprising $N = 16$ sites at a fixed value of the gain-loss parameter, $d = 2$. In the left column, the real band spectrum is plotted, while the right column displays the corresponding imaginary band spectrum. The arrangement of rows highlights the effect of different hopping conditions. The top row represents the case where the hopping integral $t_1 > t_2$, and the bottom row shows the other condition where $t_1 < t_2$.

tems show significantly enhanced currents compared to Hermitian ones. (vii) Up to a critical gain-loss threshold, the system exhibits purely real currents, and the value of this threshold varies with flux and hopping integrals, reflecting the sensitivity of the system to these parameters. (viii) At the half flux quantum, while there is a reduction in exceptional points and peaks, the current markedly increases with the gain-loss parameter in NH systems. In contrast, the current at this flux value in Hermitian systems remains close to zero. This study anticipates similar investigations to unravel complex signatures in diverse loop geometries, stimulating further research in the field.

The organization of this manuscript unfolds as follows: We commence in Sec. I with an introduction to our research. Section II details our theoretical model using the tight-binding framework and provides pertinent formulas for current computation. The results are presented and discussed across Sec. III and a comprehensive summary of our findings is presented in Sec. IV.

II. QUANTUM RING AND THEORETICAL DESCRIPTION

In this section, we provide the model Hamiltonian and description of theoretical framework applied to our system. Our chosen system is a one-dimensional ring, which

is influenced by an Aharonov-Bohm (AB) flux, denoted as ϕ . To investigate the energy spectrum and particle behavior within this ring, we utilize a tight-binding (TB) formalism. This TB Hamiltonian is specifically designed to capture the discrete nature of the lattice and the quantum effects induced by the AB flux. The structure of the Hamiltonian is presented below, forming the basis of our analysis of the physical properties.

$$H = \sum_{j(\text{odd})} (t_1 e^{i\theta} c_j^\dagger c_{j+1} + h.c.) + \sum_{j(\text{even})} (t_2 e^{i\theta} c_j^\dagger c_{j+1} + h.c.) + \sum_j \epsilon_j c_j^\dagger c_j. \quad (1)$$

Here:

- $\epsilon_j = +id$ for odd $j = 1, 5, 9, \dots$
- $\epsilon_j = -id$ for odd $j = 3, 7, 11, \dots$
- $\epsilon_j = 0$ for even $j = 2, 4, 6, \dots$

In the expression of above Hamiltonian $c_j^\dagger (c_j)$ represents the creation (annihilation) operators and j denotes the respective lattice site. The dimerized hopping integrals are signified with t_1 and t_2 and $\theta = 2\pi\phi/N$. The strength of environmental interaction is indicated by the parameter d .

We aim to study the characteristics of circular current⁸⁴⁻⁸⁷ within our system. Our focus is particularly on understanding how exceptional points and band spectra influence the current. To calculate the current, we use

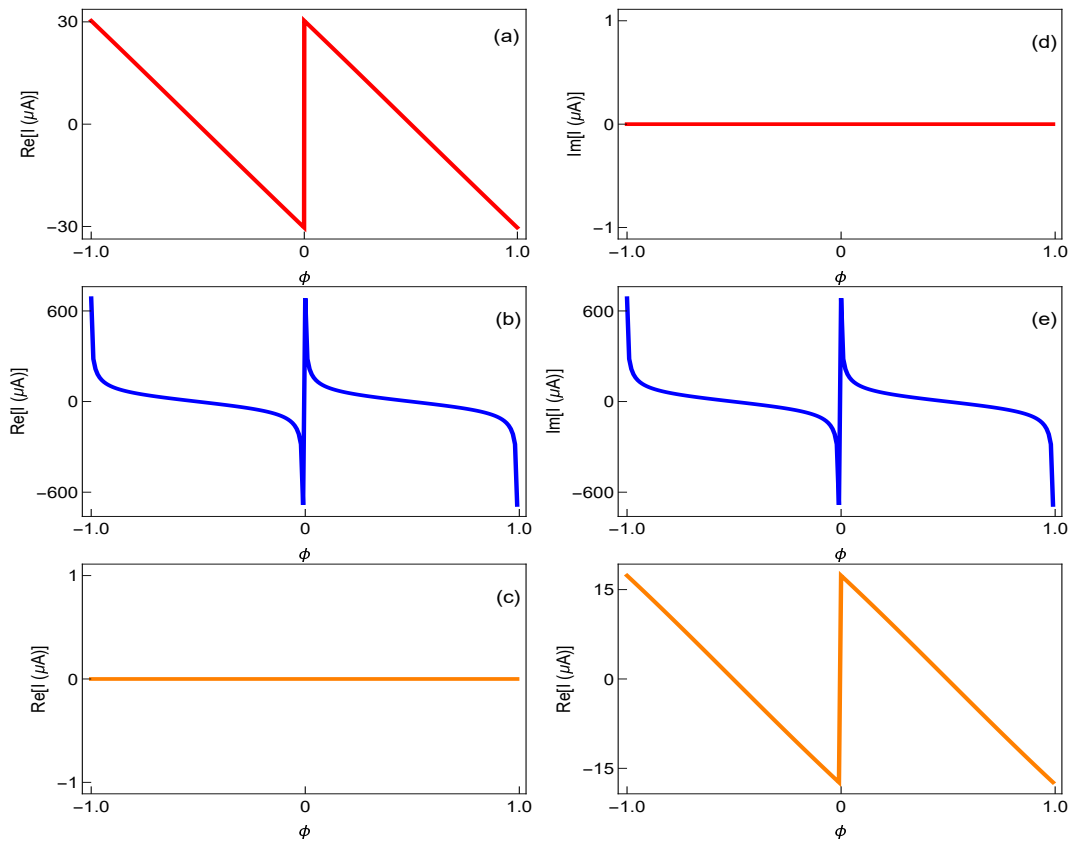


FIG. 4: (Color online). Variation of real and imaginary currents as a function of the flux ϕ for the case where the hopping integrals are equal i.e., $t_1 = t_2$. The left column illustrates the real current, while the right column displays the imaginary current. Three distinct values of the gain-loss parameter d are considered, represented by different colors: red for $d = 0$, blue for $d = 2$, and orange for $d = 4$.

the definition

$$I^{re/im} = -c \frac{\partial E_0^{re/im}}{\partial \phi} \quad (2)$$

where $E_0^{re/im}$ is the real or imaginary ground state energy and c is the constant.

Now, in the context of this NH system, we encounter both real and imaginary eigenvalues, requiring us to compute E_0 in both real and imaginary spaces. Initially, we diagonalize the Hamiltonian to obtain the real and imaginary energy eigenvalues. Subsequently, we sum the lowest N_e energy levels to determine E_0 in both real and imaginary subspaces. If E_m is the eigenvalue of m^{th} state then this process can be formulated as follows:

$$E_0^{re/im} = \sum_m^{N_e} E_m^{re/im}. \quad (3)$$

III. NUMERICAL RESULTS AND DISCUSSION

In this section, we present our numerical findings and provide insights into the circular current in our system, which is influenced by environmental interactions. For our analysis under the condition of unequal hopping integrals, the values of t_1 are maintained at 1.5 and 0.5,

while the hopping t_2 is kept at 1. When $t_1 = t_2$, we denote this condition as t and fix its value at 1. Our investigation is conducted at half-filling, allowing us to effectively study the behavior of the system. Additionally, key parameters are elaborated upon in the captions accompanying each figure, ensuring that readers have a clear understanding of the relevant conditions and context for our findings. All values of the hopping integrals and energy eigenvalues are expressed in the unit of eV while the current is measured in μA . This comprehensive approach aims to enhance the overall interpretation of the results obtained from our numerical analysis.

A. Band spectrum

We plot the band spectrum with flux in Fig. 2 for $t_1 = t_2$. The left column shows spectra with real eigenvalues, while the right column displays spectra with imaginary eigenvalues. The rows represent three different values of d , indicated by red, blue, and orange curves. At $d = 0$, the spectrum consists entirely of real eigenvalues, resembling that of a disorder-free ring. The energy levels in the real spectrum exhibit finite slopes and demonstrate high degeneracy, with some slopes canceling each other out, which limits the flow of current within the system. Increasing d to 2 results in a breakdown of the high de-

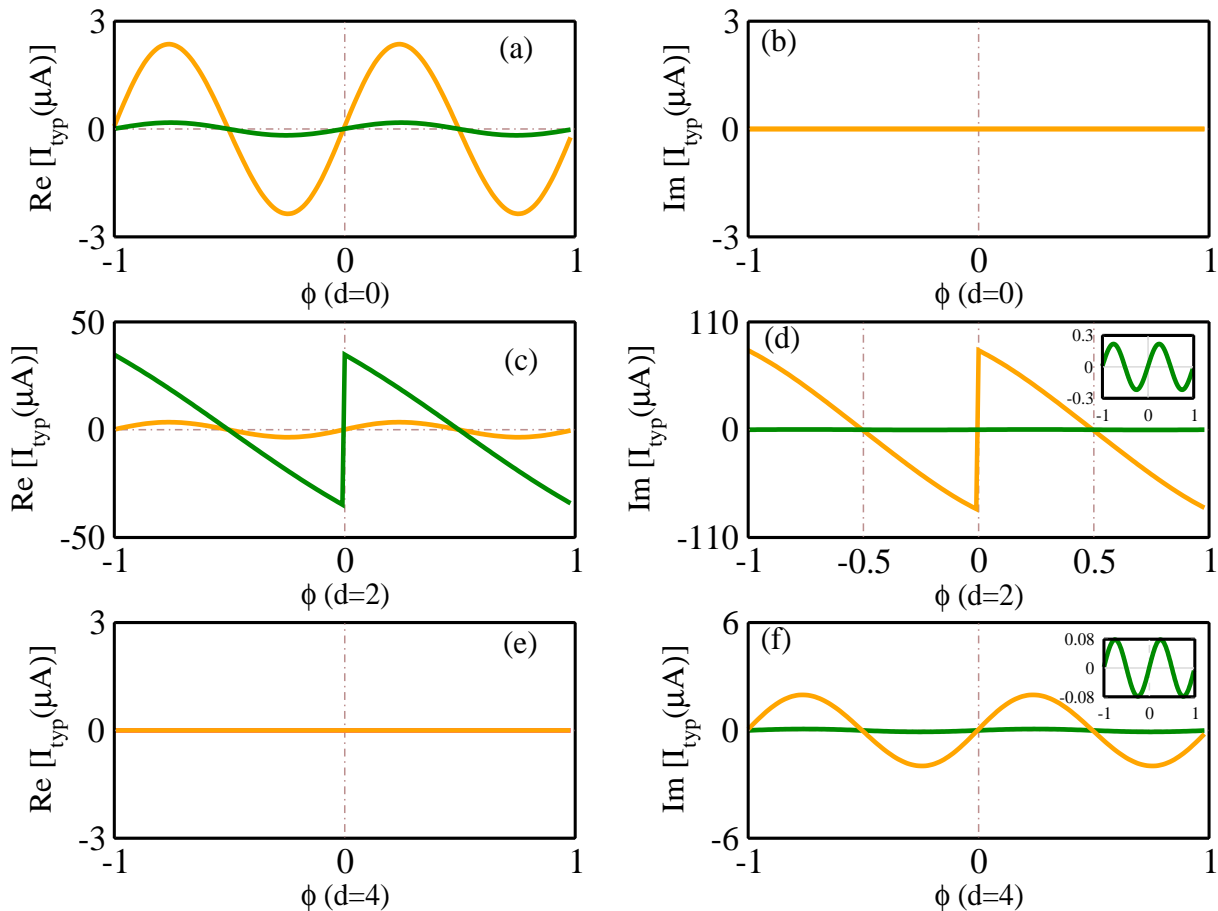


FIG. 5: (Color online). The variation of both real and imaginary current as a function of the flux ϕ , but this time for the asymmetric cases where the hopping integrals differ, specifically $t_1 > t_2$ and $t_1 < t_2$. In the left column, the real current is plotted, while the right column shows the corresponding imaginary current. The curves associated with the condition $t_1 > t_2$ are represented by orange, and those for $t_1 < t_2$ are indicated by green. These current variations are examined for three distinct values of the gain-loss parameter d , as indicated within the figure.

generacy of some energy levels. The slopes of certain levels become steeper, and the mutual cancellation of slopes appears less pronounced, suggesting a potential increase in current compared to the $d = 0$ case. When $d = 4$, the values of real eigenvalues become extremely small, nearly zero. Consequently, the spectrum is dominated by imaginary eigenvalues, leading to a scenario where the real current approaches zero.

In the right column, we observe that the imaginary eigenvalues are zero when $d = 0$, which is expected, resulting in zero imaginary current. As d increases to 2, the imaginary spectrum develops steeper slopes that generally do not cancel out across most flux regimes. This suggests the presence of a finite amount of imaginary current in this scenario. Additionally, at $d = 2$, the imaginary part of the energy spectrum looks similar with the real energy spectrum, leading to an equivalent contribution to the current from both the real and imaginary components. This correspondence between the two spectra results in identical current magnitudes in both the real and imaginary spaces. Such behavior highlights the critical role of the gain-loss parameter d in balancing the real and imaginary currents at specific value, further emphasizing

the unique characteristics of the system. The equalization of energy spectrum in both spaces is a distinctive feature that warrants deeper exploration, as it underscores the interplay between real and imaginary energies at this parameter value. Another significant observation at $d = 2$ is the emergence of doubly degenerate eigenvalues at the edges of the energy spectrum. This behavior is not limited to the spectral boundaries; within the central regions of the spectrum, we encounter nearly fourfold degenerate eigenvalues in both the real and imaginary eigen spaces. The appearance of such degenerate states in different parts of the spectrum is a remarkable and critical finding. It suggests a deeper underlying symmetry or structural characteristic in the energy landscape, particularly influenced by the gain-loss parameter d . This discovery of degeneracy, both at the spectral edges and within the bulk, provides valuable insights into the intricate behavior of the system and warrants further investigation into its physical implications, particularly in terms of current transport in NH regimes. Now, when $d = 4$, the spectrum exhibits a gapped structure with three sub-bands. The bands near the edges of the spectrum are nearly flat, resulting in very small slopes. For

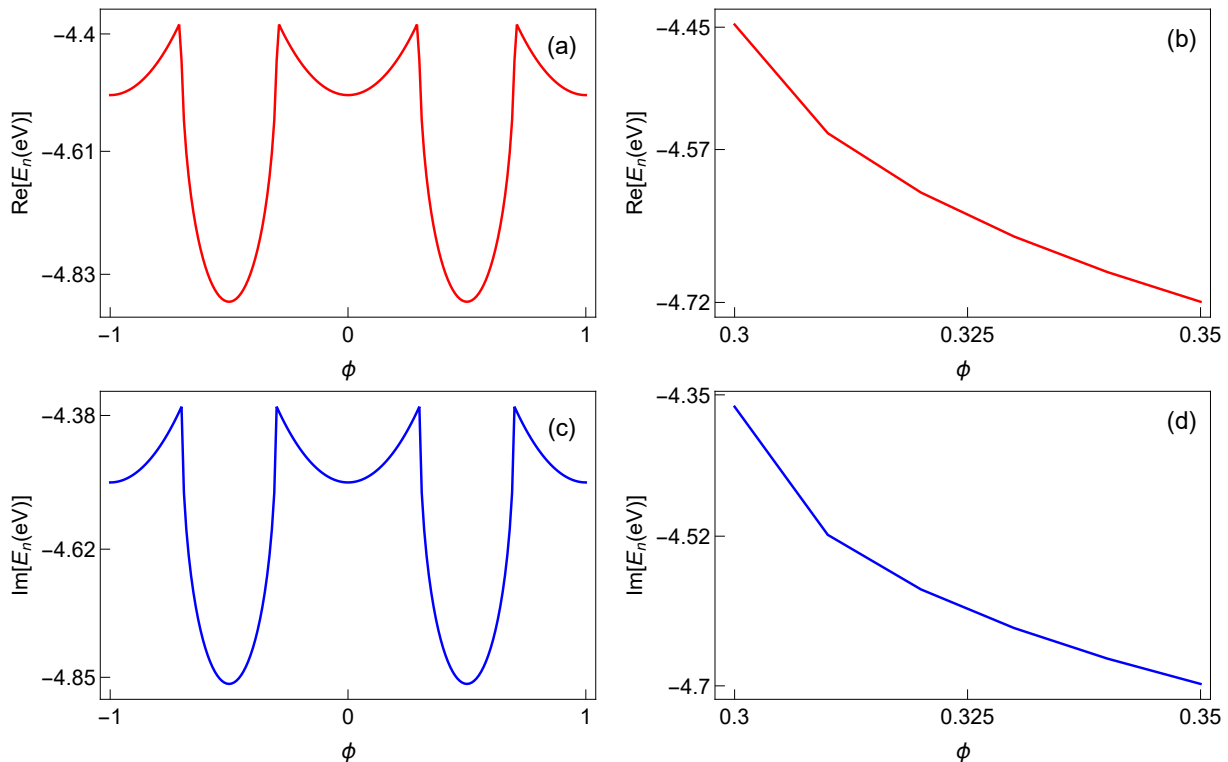


FIG. 6: (Color online). Left column: Variations in real and imaginary ground state energies as a function of flux are analyzed at specific values of the gain-loss parameter d , specifically at $d = 2.22$ for the real part and $d = 1.75$ for the imaginary part, corresponding to the first exceptional points in both the cases. Right column: To better understand and examine the slope, we thoroughly scan through a narrow range of flux to gain deeper insights, here we focus only the case where $t_1 = t_2$.

the band near the middle of the spectrum, some slopes cancel each other out, reducing the likelihood of significant current compared to the $d = 2$ case.

In Fig. 3, we present the real and imaginary energy spectra for the two cases: $t_1 > t_2$ (top row) and $t_1 < t_2$ (bottom row) at $d = 2$. These plots reveal a notable contrast and switching behavior between the real and imaginary eigenspaces depending on the relationship between the hopping integrals. For $t_1 > t_2$, we observe the formation of two distinct sub-bands in the real energy spectrum, while the imaginary energy spectrum exhibits an entirely different profile (top row). This behavior is reversed when the condition on the hopping integrals is switched from $t_1 > t_2$ to $t_1 < t_2$ (bottom row), resulting in a starkly contrasting structure in both the real and imaginary spectra. Furthermore, a column-wise comparison of the spectra shows that altering the relationship between the hopping integrals significantly changes the behavior of both the real and imaginary energy spaces. This distinct switching and contrasting behavior between the two conditions not only highlights the complex interplay between real and imaginary energy spectra but also reveals an intriguing pattern that underscores the sensitivity of the system to the relative strength of the hopping integrals.

It is important to note that sorting the real and imaginary eigenvalues separately is essential for computing current by summing energies up to specific levels for a given filling factor. This band spectrum highlights in-

triguing and contrasting non-trivial characteristics in real and imaginary currents, which vary with the parameter d that governs the strength of gain and loss.

B. Variation of current with flux

In Fig. 4, we illustrate the variation of the current as a function of flux by summing the real and imaginary eigenvalues within their respective sub-spaces and then computing the first derivative of each with respect to the flux. This approach allows us to examine how the real and imaginary components of the current respond to changes in the flux, providing a comprehensive view of the behavior of the system. The figure is organized such that the left column depicts the real current, while the right column focuses on the imaginary current, allowing for a clear comparison between these two components. From top to bottom, the rows correspond to three different values of the gain and (or) loss parameter d , specifically $d = 0$, $d = 2$, and $d = 4$. This progression enables us to observe how increasing the gain and loss parameter impacts both the real and imaginary currents at each flux value. Importantly, these calculations are performed for the symmetric hopping condition, where $t_1 = t_2$. This choice ensures that any changes in the current behavior can be attributed directly to variations in the flux and the parameter d , rather than to asymmetry between the hopping integrals.

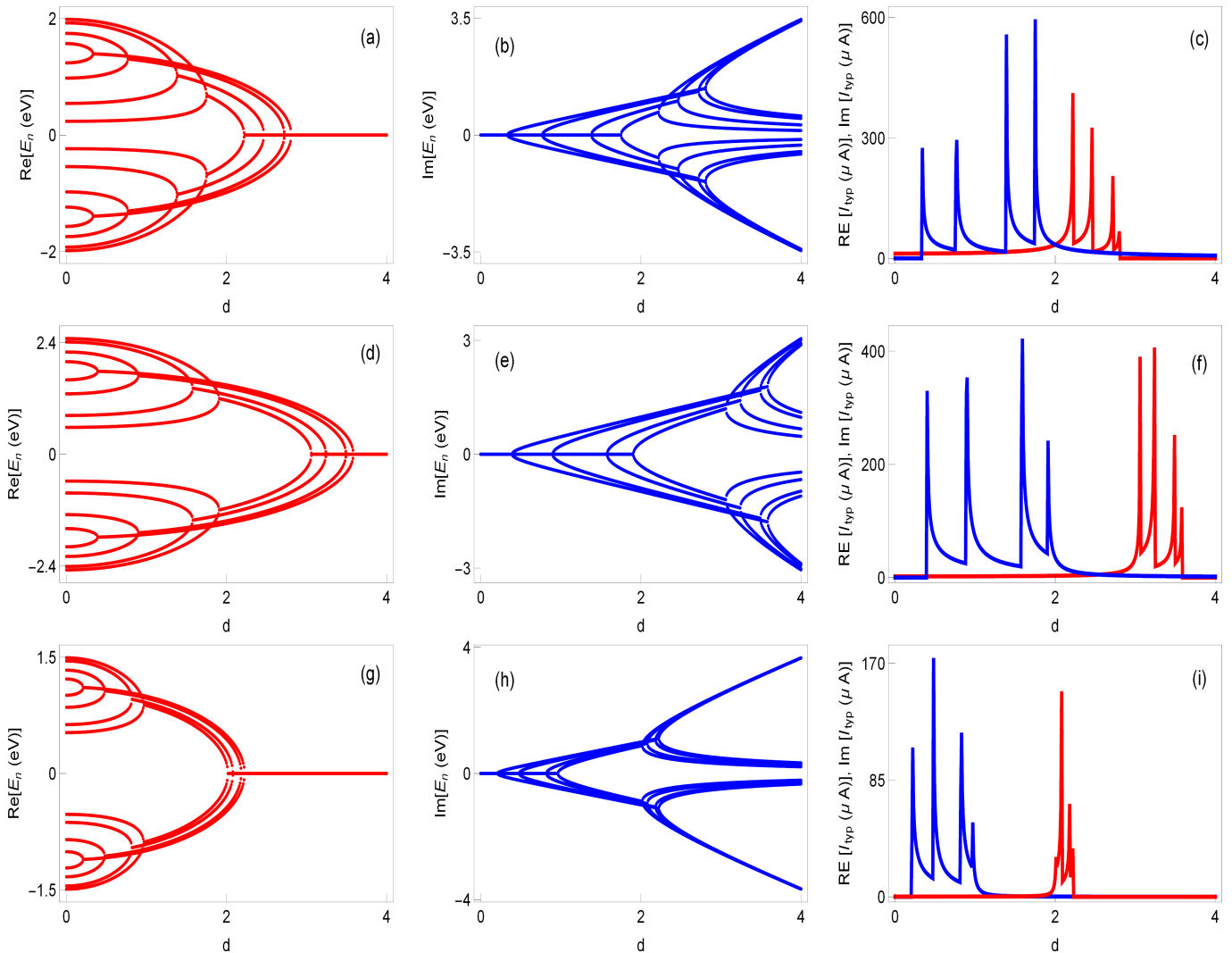


FIG. 7: (Color online). The figure presents the variations of both the real and imaginary eigenvalues, along with the currents, as a function of the gain-loss parameter d for three distinct configurations of the hopping integrals: $t_1 = t_2$ (top row), $t_1 > t_2$ (middle row), and $t_1 < t_2$ (bottom row). In this representation, the red curves denote the real components, while the blue curves illustrate the imaginary components of both the energy bands and the currents. The analysis is conducted with a fixed flux value of $0.3\phi_0$, ensuring consistency across the three scenarios and the system size is kept at $N = 16$.

Focusing on the real current, we observe a gradual and steady increase as the gain and loss parameter, d , is increased. This trend is in line with the behavior seen in the energy band spectrum for real eigenvalues, where the real eigenenergies grow as d increases. However, as d reaches the value of 4, the real current diminishes to zero. At this point, the real eigenenergies of the system become negligible, essentially vanishing. This phenomenon is clearly represented by the orange curve in the plot, illustrating how the real current is directly tied to the real eigenvalue spectrum of the system and becomes insignificant as the real part of the eigenspectrum fades away at higher values of d .

Turning our attention to the right column of the figure, we can see that the imaginary current behaves differently. When $d = 0$, the imaginary current is zero, which is expected as the system exhibits a completely real eigenspectrum in this regime. As d increases, the

imaginary current begins to rise, reflecting the increasing contribution of imaginary eigenvalues. However, this rise is not indefinite. At $d = 4$, we notice a reduction in the imaginary current. This oscillatory pattern in the current is largely driven by the interaction between physical gain and loss, which occurs at alternating odd lattice sites. Interestingly, even though the real energy spectrum becomes almost entirely imaginary at $d = 4$, this does not lead to a continuous enhancement of the imaginary current. Instead, the current follows a non-linear behavior due to the complex effects of gain and loss. The parameter d influences the hopping process, and once a certain threshold is surpassed, localization effects may arise. This suggests that while the gain and loss terms contribute to the current, they also introduce a limit beyond which further increment of d does not result in enhanced current flow. Rather, they might lead to the suppression of transport due to the onset of lo-

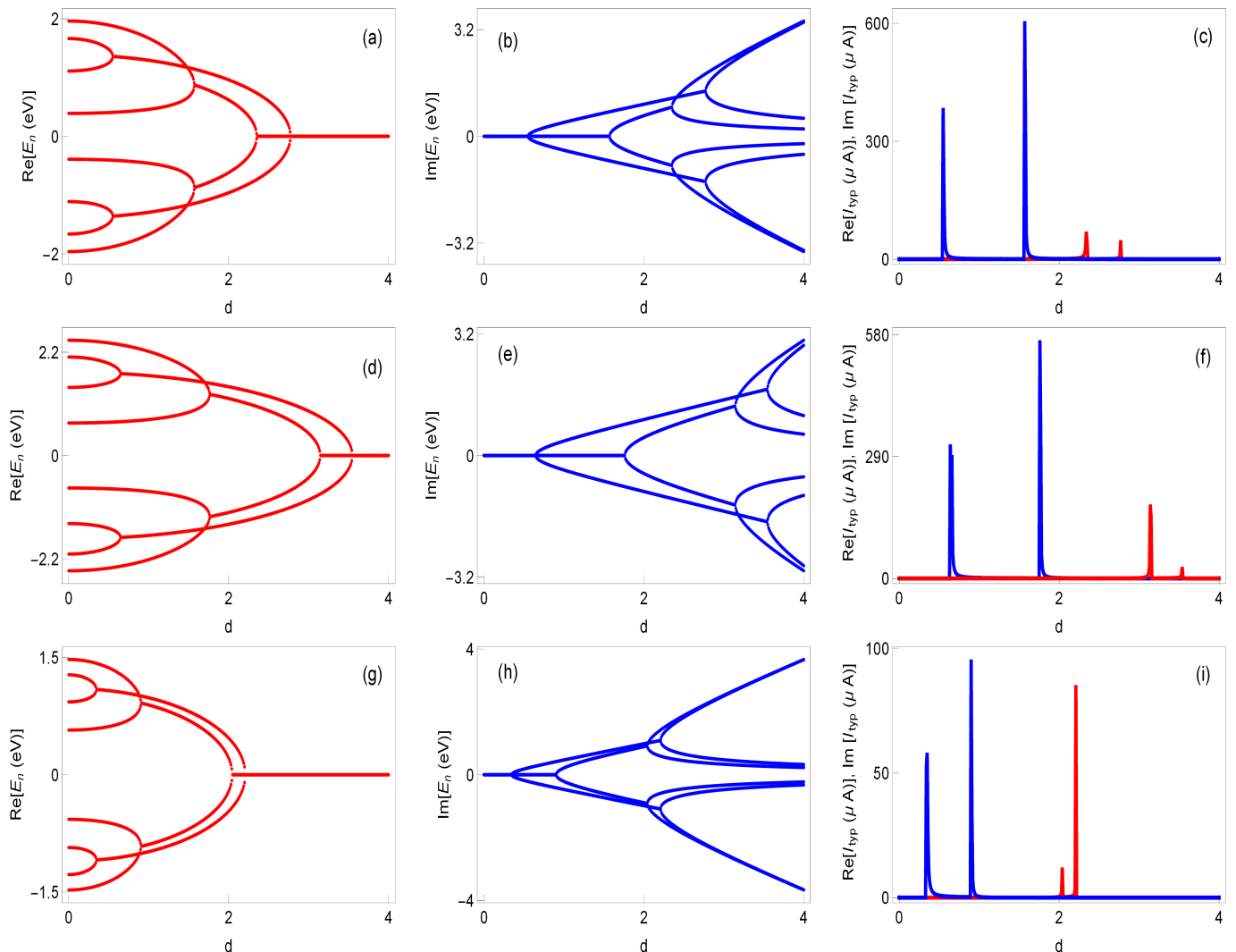


FIG. 8: (Color online). The figure illustrates the variation in the energy bands and corresponding currents as a function of the gain-loss parameter d , but with the flux now set at $\phi = 0.5\phi_0$. As in the previous plot, the analysis is also performed for three distinct configurations of the hopping integrals: $t_1 = t_2$, $t_1 > t_2$, and $t_1 < t_2$. The real and imaginary components of the energy band spectrum and corresponding currents are depicted using red and blue curves, respectively, maintaining the same system size of $N = 16$, as shown in the previous plot.

calization effects, which restrict the mobility of particles in the system and thereby reduce the magnitude of the current.

An additional significant observation from Fig. 4 is the intersecting point where the real and imaginary currents converge, specifically at $d = 2$. This is a key result, indicating that at this particular value of the gain and loss parameter d , the magnitudes of both the real and imaginary components of the current are equal. This phenomenon is distinctly visible in the figure, highlighting the intersection of the two current profiles, where the contributions from real and imaginary eigenvalues appear to be balanced. The equivalence of the real and imaginary currents at $d = 2$ can be further clarified by examining the underlying relationship between the energy spectrum of the system and the applied flux. As the energy bands evolve with flux for this value of d , it appears that the interplay between real and imaginary eigenvalues becomes

symmetrical, resulting in the matching currents. This behavior suggests that at $d = 2$, the system reaches a unique point of balance between the gain and loss effects introduced at alternate lattice sites. Such a scenario is particularly important because it underscores the critical role that the parameter d plays in dictating the transport properties. This observation not only contributes to our understanding of the role of d in modulating the current but also hints at potential symmetry or resonance effects that arise at intermediate values of the gain and loss parameter, further enriching the overall picture of transport in NH systems.

If we closely examine Fig. 5, an intriguing pattern emerges. In this figure, we plot the current as a function of flux, where the orange and green curves represent the cases $t_1 > t_2$ and $t_1 < t_2$, respectively. At $d = 0$, the real current for $t_1 > t_2$ exceeds that of $t_1 < t_2$, suggesting that the system with stronger hopping integral

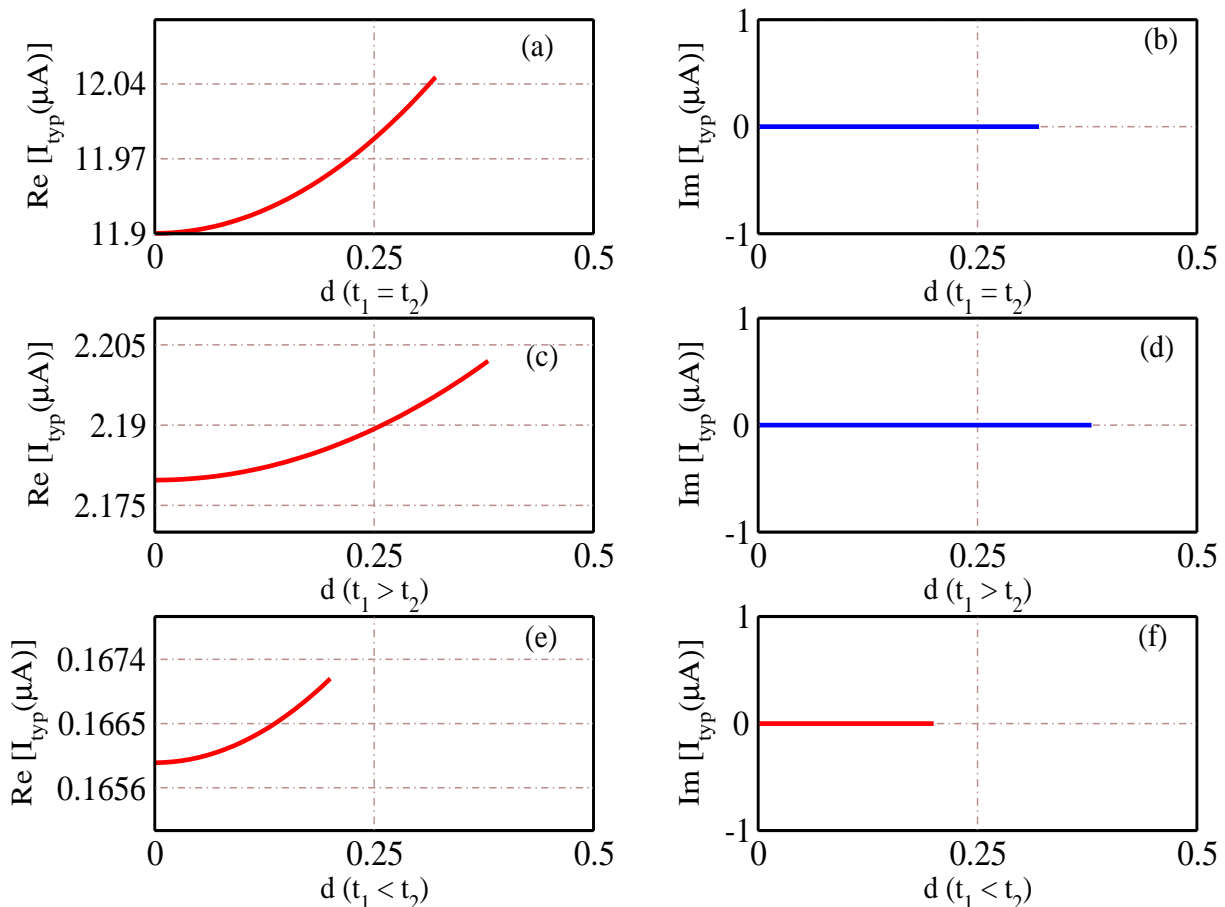


FIG. 9: (Color online). This figure displays how the real and imaginary currents vary with respect to the gain-loss parameter d , extending up to the threshold value, at which the imaginary current reaches zero. This analysis has been conducted under specific conditions at a flux value of $0.3\phi_0$ and for a system size of $N = 16$.

(t_1) displays a more significant transport response. However, once we introduce the NH parameter d and set it to $d = 2$, the situation reverses. In this case, the current for $t_1 < t_2$ becomes greater than for $t_1 > t_2$, highlighting a shift in the transport characteristics driven by the gain and loss parameter. What makes this even more intriguing is that in the imaginary current space, the behavior is inverted at $d = 2$. In other words, while the real current for $t_1 < t_2$ dominates, the imaginary current shows the opposite trend, with $t_1 > t_2$ exhibiting a larger imaginary current than $t_1 < t_2$. This inversion points to a non-trivial interaction between the real and imaginary components, suggesting that such type of gain and loss in NH systems can lead to distinct transport signatures depending on the domain being considered. Moreover, in imaginary space this behavior persists even when d is further increased to $d = 4$, where the real current has diminished to zero. Even at this value, the imaginary current for $t_1 > t_2$ continues to exceed that for $t_1 < t_2$, indicating that the switching behavior between different hopping correlations, as modulated by the parameter d , is indeed an interesting feature. These recurring transitions between different hopping regimes as d varies are undoubtedly significant findings.

These plots play a pivotal role in demonstrating how

the current evolves in response to changes in the gain and loss parameters, offering a clear visualization of their interaction and influence on the transport properties of the system. By systematically calculating the current at a fixed flux and analyzing its variation with d for both the real and imaginary components, we gain valuable insights into the underlying physical mechanisms. This approach allows for a more comprehensive understanding of the NH effects on current behavior. The following subsection will provide a detailed analysis and discussion of these significant observations delivers deeper understanding on the complex relationship between the gain-loss pattern and the current in various regimes.

C. Variation of ground state energy with flux

To better understand the behavior of current at exceptional points, we investigate the variation in both the real and imaginary components of the ground state energies (as shown in the left column of Fig. 6) with respect to the flux, focusing on the values of d near the first exceptional point for a specific case where $t_1 = t_2$. This analysis is presented in Fig. 6. To improve clarity, we limit the flux range in our plots to a very narrow window (right column

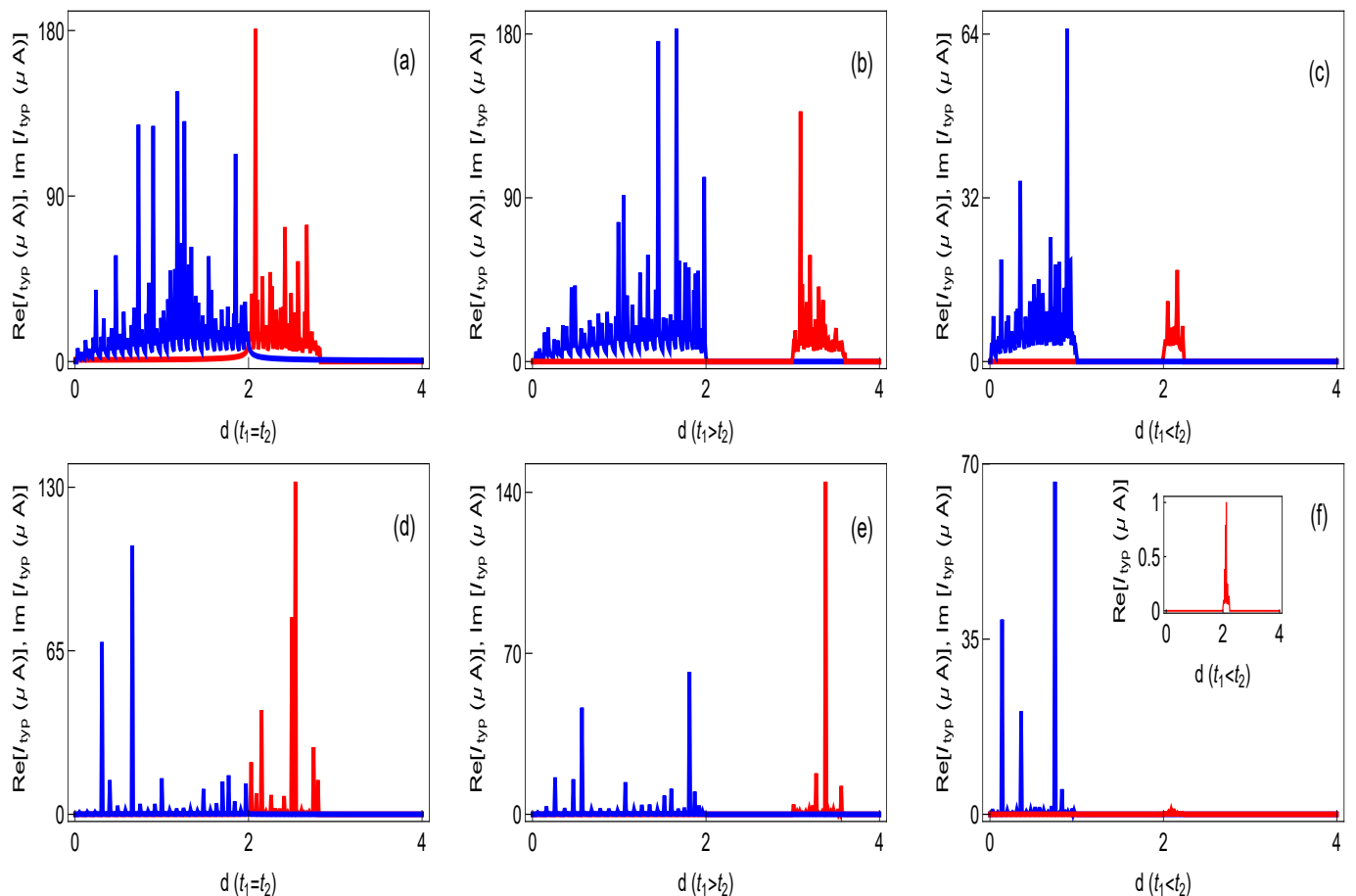


FIG. 10: (Color online). The figure presents the variation of real (represented in red) and imaginary (depicted in blue) currents as a function of the gain-loss parameter d for a larger system size of $N = 200$. This analysis is conducted at two flux values, $0.3\phi_0$ (top row) and $0.5\phi_0$ (bottom row), and it aims to illustrate the consistency of current behavior with system size.

of Fig. 6), allowing for a more detailed examination of the ground state energy behavior. The results indicate that the ground state energies change continuously with flux, marked by sharp slopes. These steep gradients have a pronounced impact on the current at exceptional points, significantly enhancing both the real and imaginary components of the current as d is varied. This observation highlights the critical influence of the slope steepness on current, showing how the parameter d plays a vital role in amplifying both the real and imaginary parts of the current in the vicinity of these exceptional points.

D. Variation of energy and typical current with d

We present the variation of real and imaginary eigenvalues and corresponding typical currents at a constant flux with the strength of the gain and loss parameter in Fig. 7. The three different rows represent three different conditions between the hopping integrals respectively. Upon examining the energy spectrum, we observe that the real eigenvalues bifurcate at lower values of d and approach the zero energy axis at higher d . Conversely, the imaginary eigenvalues exhibit opposite behavior to the real ones. Exceptional points are identified in both the

real and imaginary spectra. Given these characteristics of the energy spectrum, it is intriguing to investigate the behavior of the current at these exceptional points on the zero energy axis. We compute the current at a fixed flux of $0.3\phi_0$, as noted in the figure caption, and plot its variation with respect to the gain and (or) loss parameter d , highlighting the relationship between d and current. For the real current, we observe that it is lower at the bifurcation points away from the zero energy axis. As the energy spectrum approaches and intersects the zero energy axis, the current gradually increases, exhibiting peaks at four exceptional points, and diminishes when the real energies become negligible and approach zero.

Conversely, the imaginary current displays an opposite pattern when plotted against d . It shows peaks at the four exceptional points on the zero energy axis and decreases as the spectrum bifurcates away from this axis, diverging outward. This contrasting behavior of the real and imaginary currents is clearly illustrated in Fig. 7. Thus, we can say that the diverging nature of the energy spectrum from the zero energy axis generally leads to a reduction in the current, regardless of the presence of exceptional points away from the zero energy axis. Conversely, the converging tendency of the energy spectrum towards the zero energy level enhances

the current. Moreover, the exceptional points lying precisely on the zero energy axis exhibit maximum sensitivity, significantly enhancing the current and manifesting as peaks at those points. When correlations between the hopping amplitudes are introduced ($t_1 \neq t_2$), the energy spectrum experiences a significant shift relative to the previous scenario where $t_1 = t_2$. This alteration leads to a notable change in the distance between the exceptional points in the system, which directly impacts the behavior of the current. Specifically, the spacing between the points where the imaginary current decreases and the real current increases, as seen in the current spectra with respect to the gain and (or) loss parameter d , becomes wider. This widening occurs for both $t_1 > t_2$ and $t_1 < t_2$ cases, suggesting that the correlation between the hopping terms plays a crucial role in altering the response of the system.

In these cases, the real current continues to increase over a larger range of the parameter d , while the suppression of the imaginary current is also more spread out. This broader separation between the decrement of the imaginary current and the enhancement of the real current signifies a more pronounced impact of the exceptional points on the transport properties of the system. The introduction of asymmetry between the hopping amplitudes not only shifts the position of the exceptional points but also alters the manner in which the currents evolve, giving rise to an extended region where the real current is amplified. By tuning the relationship between t_1 and t_2 , one can systematically modify the transport properties, thereby offering a potential method for enhancing the real current while simultaneously suppressing the imaginary component. This ability to control the interplay between the real and imaginary parts of the current highlights the versatility of the system and its sensitivity to changes in hopping correlations.

In Fig. 8, we present the energy and current as functions of the gain and (or) loss parameter d for a fixed flux of $\phi = 0.5\phi_0$. Notably, this figure reveals a substantial reduction in the number of exceptional points compared to other flux values, which, in turn, leads to fewer pronounced peaks in both the real and imaginary components of the current. A key observation here is that, in the Hermitian case, the current at $\phi = 0.5\phi_0$ tends to approach zero, indicating minimal transport at this flux. However, under NH conditions, we observe a significant non-zero current, despite the reduced number of peaks relative to other flux values. This behavior underscores the impact of NH pattern in maintaining and even enhancing current at specific flux values, which would otherwise show minimal current in Hermitian systems. Additionally, this phenomenon is consistently observed across all three cases involving different relations between the hopping integrals, although the position and behavior of the exceptional points vary with each case. These results suggest that while the number of exceptional points may be reduced for $\phi = 0.5\phi_0$, the NH characteristics still facilitate substantial current, highlighting the robustness of current enhancement in such systems despite variations in flux and hopping parameters.

As shown in Fig. 9, we observe that the real compo-

nent of the current exhibits a noticeable increase as the parameter d is gradually increased. This upward trend continues until d reaches a specific threshold, which we refer to as the critical value d_c . Beyond this point, the behavior of the current may change, indicating the significance of d_c in governing the response. This critical value marks a key transition in the behavior of the current as d is varied, where the imaginary part of the current reaches zero. Within this range, the system maintains a completely real behavior, and the increase in d from its initial value leads to a significant amplification of the real current. Remarkably, under these conditions, the magnitude of current can exceed that of a perfectly ordered lattice without any disorder. This phenomenon is consistently observed across all three configurations of the hopping integrals, though the threshold value d_c varies between these cases. The presence of such physical mechanisms involving gain and loss underpins the existence of a purely real energy spectrum up to this critical value of d , allowing for substantial enhancement of the current. This observation highlights the impact of the such type of physical gain and loss on its transport properties.

In Fig. 10, we present the variation of both real and imaginary components of the current with respect to the gain and (or) loss parameter d , under three different conditions involving the hopping integrals. The results are shown for two distinct flux values: $\phi = 0.3\phi_0$ in the top row and $\phi = 0.5\phi_0$ in the bottom row, all within the context of a large 200-site ring. Despite the increase in system size, the distinct behavior of real and imaginary currents for the varying hopping conditions remains clearly evident across both flux values. This highlights the robustness of the behavior of current in NH systems, even in larger lattices. Moreover, for $\phi = 0.5\phi_0$ (bottom row), we observe a decrease in the number of peaks in the current, which is in line with the trends previously identified in smaller system sizes. This indicates that the response of the system, particularly the reduction in peaks at this specific flux value, scales consistently with size. Another noteworthy observation is the substantial magnitude of the current, even for the large site ring. This enhancement in current, despite the larger lattice size, is a crucial finding and demonstrates that the system retains significant transport properties as the lattice expands. The figure provides clear visual confirmation of these trends, emphasizing the persistence of these distinctive current features in both real and imaginary components for larger quantum systems.

E. Variation of d_c with ϕ and hopping parameters

In this work, we introduce a parameter, d_c , which denotes the critical value of d up to which the imaginary current remains zero. Figure 11 illustrates how d_c varies as a function of ϕ and the hopping integrals. The subplot in Fig. 11(a) specifically depicts the relationship between d_c and the flux for three distinct conditions involving the hopping integrals. The red, green, and blue curves correspond to $t_1 = t_2$, $t_1 > t_2$, and $t_1 < t_2$, respectively. It is evident from the figure that d_c is higher when $t_1 > t_2$

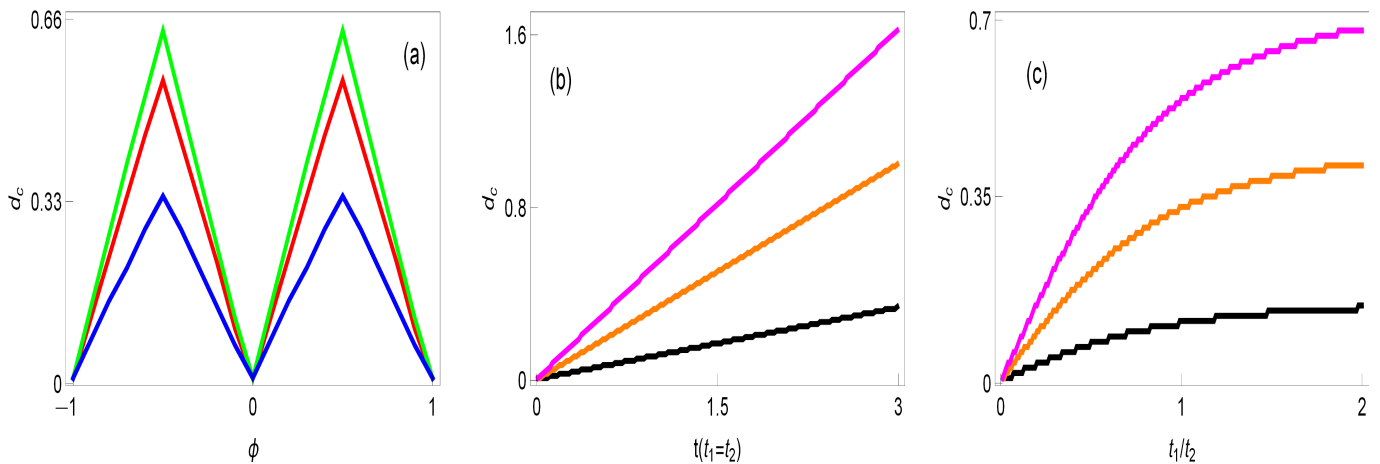


FIG. 11: (Color online). Variation of d_c with flux ϕ , hopping $t(t_1 = t_2)$, and the ratio t_1/t_2 is presented in the figure. In subplot (a), the curves colored red, green, and blue correspond to the scenarios where $t_1 = t_2$, $t_1 > t_2$, and $t_1 < t_2$, respectively. Conversely, in the other subplots, the plots in black, orange, and magenta represent the cases for $\phi = 0.1$, $\phi = 0.3$, and $\phi = 0.5\phi_0$, respectively.

compared to the other cases. Another key observation is that d_c reaches its maximum when $\phi = 0.5\phi_0$, and then decreases linearly, reaching zero for integer values of flux. This indicates that for $\phi = 0.5\phi_0$, the system can sustain higher values of d before the onset of any imaginary current. The interaction between the hopping integrals, the physical gain and loss mechanisms, and the applied flux collectively influence the system, resulting in these observed characteristics. This analysis not only highlights the dependency of d_c on the interplay between these factors but also provides valuable insights into the critical thresholds beyond which the imaginary current emerges in the system.

The occurrence of this specific behavior in d_c suggests that the location of the first exceptional point along the zero-energy axis can be effectively controlled by varying the flux, as well as by adjusting the conditions between the hopping integrals. This indicates that the exceptional point, which marks a critical transition, is not fixed but can be shifted depending on these external parameters. By manipulating the flux and the relationship between t_1 and t_2 , the critical point can be fine-tuned, offering a deeper understanding of how external factors influence the emergence of exceptional points. This tunability is significant as it provides a potential pathway for experimental control over quantum systems exhibiting NH characteristics.

Subplot Fig. 11(b) illustrates how d_c varies as a function of the hopping parameter when $t_1 = t_2 = t$, for three distinct flux values ($\phi = 0.1\phi_0$, $0.3\phi_0$, and $0.5\phi_0$), represented by black, orange, and magenta curves, respectively. From this plot, it is evident that d_c exhibits a linear increase with increasing t . Furthermore, the value of d_c remains consistently higher for $\phi = 0.5\phi_0$ compared to the other flux values across all hopping strengths. This behavior suggests that at very low hopping values, the first exceptional point where the system undergoes a transition into a NH regime begins near zero. As the hopping parameter t increases, the location of the excep-

tional point shifts to higher values of d . In other words, stronger hopping allows the system to support larger values of d before the onset of imaginary current, with the flux value playing a significant role in determining the precise magnitude of d_c . The dependence of d_c on both the hopping strength and flux highlights the intricate interplay between these parameters in controlling the transition of the system to the exceptional point.

The variation of d_c with the ratio t_1/t_2 is presented in subplot Fig. 11(c), where the color-coded curves represent different flux values, as indicated in the earlier subplots. This plot reveals an approximately step-like behavior in d_c as t_1/t_2 changes. Notably, the position of the first exceptional point shows minimal variation for small changes in t_1 . The step-like pattern is particularly pronounced for $\phi = 0.1\phi_0$, especially at higher values of t_1 . This suggests that under certain flux conditions, the system exhibits a more distinct transition in d_c as the hopping ratio is adjusted, with the influence of ϕ being most significant for smaller flux values. This behavior underscores the sensitivity of the exceptional point to the interplay between hopping integrals and flux, revealing that in certain regimes, the system remains robust to small changes in t_1 , while in others, the response is more pronounced. This step-like nature could have implications for controlling and fine-tuning the transition points in experimental setups.

F. Variation of current with N

Figure 12 demonstrates how the system size influences the current specifically in the half-filled scenario. The figure is structured with the real current shown in the left column and the imaginary current in the right column, while the three rows correspond to different configurations of the hopping integrals. Within each graph, the red, green, and blue curves represent varying values of d , as elaborated upon in the figure caption.

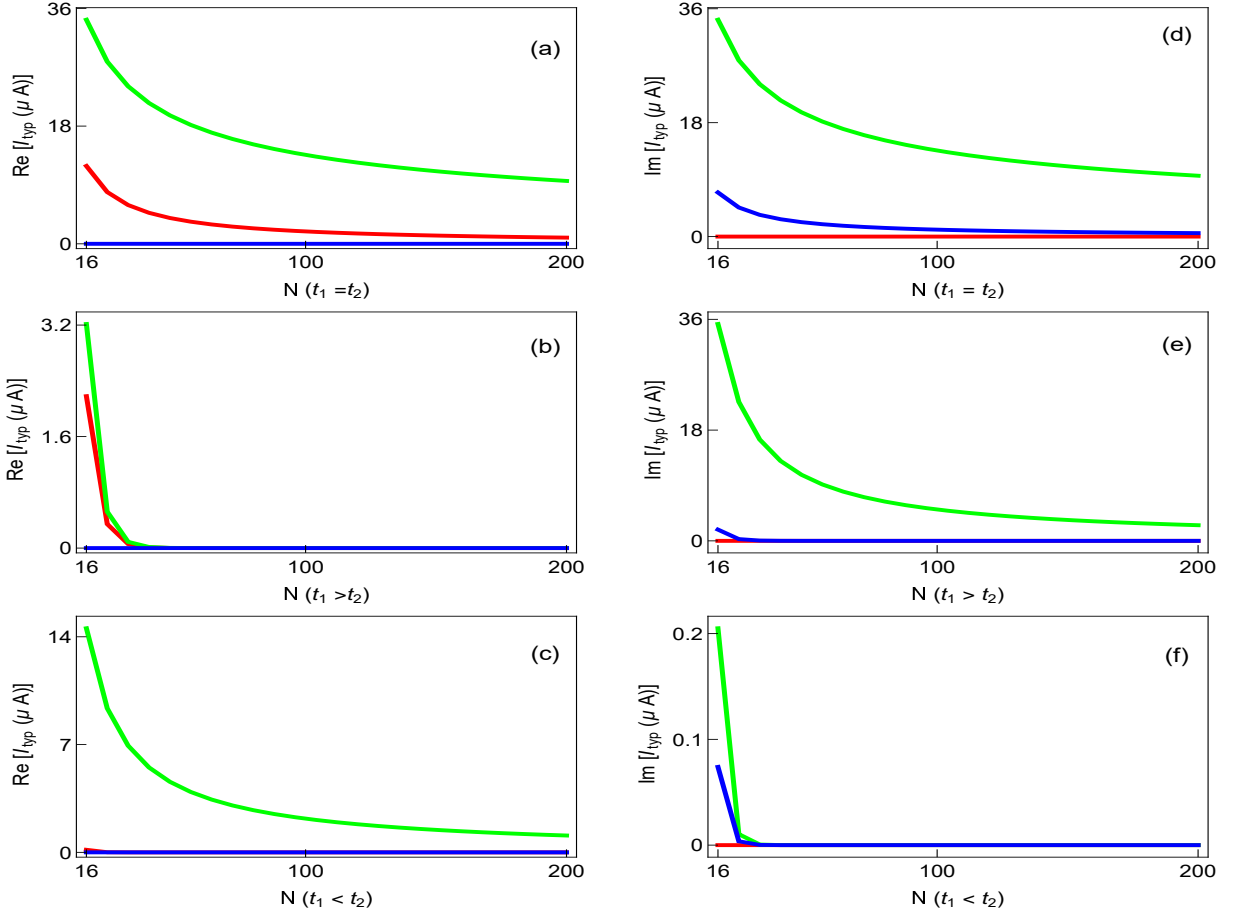


FIG. 12: (Color online). The figure provides a detailed depiction of the variations in real and imaginary currents as they relate to system size, specifically under the condition of half-filling. This analysis is performed across three distinct configurations regarding the hopping integrals. In the individual plots, the curves are color-coded, with red representing $d = 0$, green indicating $d = 2$, and blue corresponding to $d = 4$. The results are shown by varying the ring size in a wide range, and the flux is maintained at a constant value of $\phi = 0.3\phi_0$.

It is evident from the figure that both the real and imaginary currents decrease as the system size increases, which is indicative of the typical behavior of persistent current in larger systems. This decrease in current with increasing system size has been well-documented in prior studies and is reaffirmed here. A closer look reveals that as d is increased from 0 to 2, there is a noticeable rise in the current. However, when d is increased beyond 2, the current begins to decrease again, showing a non-linear relationship between the current and d . Moreover, an intriguing pattern emerges when comparing the real and imaginary currents under varying conditions of the hopping integrals. For $t_1 > t_2$, the real current is consistently smaller than the imaginary current. On the other hand, when $t_1 < t_2$, this relationship is reversed, with the real current becoming larger than the imaginary current. This inversion in behavior can be explained by the interaction of the gain and loss factors at the odd lattice sites, in conjunction with the specific correlation between the hopping integrals.

Overall, these findings highlight the complex and non-linear nature of the dependence of current on both the system size and the parameter d . The findings are consis-

tent with earlier theoretical work on persistent current, while also uncovering new details about the behavior of real and imaginary currents under different conditions. This comprehensive study of how the current varies with system size and other parameters provides a more profound understanding of the underlying physical mechanisms involved.

IV. CONCLUSIONS

The primary objective of this study is to investigate the behavior of circular currents and to determine how these currents can be enhanced by carefully tuning parameters that govern physical gain and loss also with the correlations between the hopping integrals. This exploration also takes into account the influence of environmental interactions. By strategically introducing gain and loss components within the ring system, we observe that both the real and imaginary spectra dominate within a particular range of these parameters, leading to the full realization and amplification of the current up to a certain threshold. The emergence of exceptional points,

along with the shifting characteristics of the energy band spectrum, plays a pivotal role in significantly amplifying the current. Our approach employs a tight-binding model to simulate the system, allowing us to diagonalize the Hamiltonian and extract both the real and imaginary parts of the eigenenergies. The current is then calculated by differentiating the eigenvalues with respect to flux. The analysis reveals that the gain and loss parameters, when finely tuned, can push the system into a regime where the real current is fully enhanced, and the imaginary component either vanishes or complements the real spectrum, depending on the range of parameters. The presence of exceptional points, which mark the transition between different physical regimes, is crucial in this process. These points influence the band structure in such a way that they can substantially increase the current at specific parameter values. The behavior of the band spectrum whether it converges or diverges also directly impacts the magnitude of the current, with converging spectra leading to an enhancement in the current. The key findings of our study can be summarized as follows:

- At smaller values of the gain-loss parameter (d), the real band spectrum dominates the behavior of the system, gradually diminishing towards zero as d increases for the case where the hopping integrals are equal ($t_1 = t_2$). In contrast, the imaginary band spectrum follows an inverse trend, becoming more prominent as d grows larger.
- When $d = 2$, both the real and imaginary eigenspectra display similar characteristics, with several eigenvalues exhibiting double and fourfold degeneracies. However, when d increases to 4, this fourfold degeneracy is broken in imaginary eigenspace, leaving only doubly degenerate eigenvalues.
- A key observation is that the behavior of the real and imaginary bands reverses depending on the condition of the hopping integrals ($t_1 > t_2$ or $t_1 < t_2$) at certain specific values of d . This switching behavior offers an interesting insight into how the system transitions between different regimes as d varies.
- At $d = 2$, for the case of $t_1 = t_2$, the real and imaginary currents are identical. However, as d changes, the system displays a switching behavior in the current between the

conditions of $t_1 > t_2$ and $t_1 < t_2$, for both real and imaginary eigenspaces. This indicates a significant correlation between the hopping integrals and the gain-loss parameter.

- The sensitivity increases as the real or imaginary energy spectrum converges or diverges near the zero-energy axis. This sensitivity is particularly pronounced when exceptional points lie near the zero-energy axis, where the system becomes especially responsive to changes in parameters.
- The number of exceptional points located on the zero-energy axis corresponds to the number of peaks observed in the real and imaginary current spaces. The current reaches its maximum near these exceptional points, where the spectra converge. Interestingly, there is an inverse relationship between the real and imaginary currents: when one peaks, the other dips.
- When the hopping integrals differ ($t_1 \neq t_2$), the spacing between the decrease in imaginary current and the increase in real current becomes larger compared to the case where $t_1 = t_2$. This behavior remains consistent even when the system size is increased, suggesting a significant characteristic of the model.
- A reduction in the number of exceptional points and corresponding peaks is observed at $\phi = 0.5\phi_0$, while the current increases significantly with the gain-loss parameter in NH systems, compared to Hermitian systems, even at $\phi = 0.5\phi_0$.
- Up to a critical value of the gain-loss parameter (d_c), the system exhibits a purely real current, with the imaginary current becoming completely zero. Upto this threshold, the magnitude of the real current can be enhanced by adjusting the same parameter. Importantly, the value of d_c changes based on the relationship between the hopping integrals.
- Finally, the variation of d_c as a function of flux, hopping integrals, and the correlation between the hopping integrals reveals several intriguing properties. These findings point to a complex interplay between the physical parameters and sensitivity, which are discussed in detail in subsequent sections.

* Electronic address: souvikroy138@gmail.com

† Electronic address: santanu.maiti@isical.ac.in

¹ C. M. Bender and S. Boettcher, Phys. Rev. Lett. **80**, 5243 (1998).

² C. M. Bender, M. Gianfreda, S. K. Özdemir, B. Peng, and L. Yang, Phys. Rev. A **88**, 062111 (2013).

³ C. M. Bender, Rep. Prog. Phys. **70**, 947 (2007).

⁴ K. G. Makris, R. El-Ganainy, D. N. Christodoulides, and Z. H. Musslimani, Phys. Rev. Lett. **100**, 103904 (2008).

⁵ S. Klaiman, U. Günther, and N. Moiseyev, Phys. Rev. Lett. **101**, 080402 (2008).

⁶ S. Longhi, Phys. Rev. Lett. **103**, 123601 (2009).

⁷ O. Bendix, R. Fleischmann, T. Kottos, and B. Shapiro, Phys. Rev. Lett. **103**, 030402 (2009).

⁸ T. Kato, Springer, 2nd edition (1995).

⁹ A. Regensburger, C. Bersch, M. -A. Miri, G. Onishchukov,

D. N. Christodoulides, and U. Peschel, Nature **488**, 167 (2012).

¹⁰ S. A. H. Gangaraj and F. Monticone, Phys. Rev. Lett. **121**, 093901 (2018).

¹¹ C. E. Rüter, K. G. Makris, R. El-Ganainy, D. N. Christodoulides, M. Segev, and D. Kip, Nat. Phys. **6**, 192 (2010).

¹² T. Eichelkraut, R. Heilmann, S. Weimann, S. Stützer, F. Dreisow, D. N. Christodoulides, S. Nolte, and A. Szameit, Nat. Comm. **4**, 2533 (2013).

¹³ J. M. Zeuner, M. C. Rechtsman, Y. Plotnik, Y. Lumer, S. Nolte, M. S. Rudner, M. Segev, and A. Szameit, Phys. Rev. Lett. **115**, 040402 (2015).

¹⁴ T. E. Lee, Phys. Rev. Lett. **116**, 133903 (2016).

¹⁵ M. Li, X. Ni, M. Weiner, A. Alú, and A. B. Khanikaev, Phys. Rev. B **100**, 045423 (2019).

- ¹⁶ L. E. F. F. Torres, *J. Phys.: Mater.* **3**, 014002 (2020).
- ¹⁷ C. Dembowski, H.-D. Gräf, H. L. Harney, A. Heine, W. D. Heiss, H. Rehfeld, and A. Richter, *Phys. Rev. Lett.* **86**, 787 (2001).
- ¹⁸ A. A. Mailybaev, O. N. Kirillov, and A. P. Seyranian, *Phys. Rev. A* **72**, 014104 (2005).
- ¹⁹ T. Goldzak, A. A. Mailybaev, and N. Moiseyev, *Phys. Rev. Lett.* **120**, 013901 (2018).
- ²⁰ M. K. Oberthaler, R. Abfalterer, S. Bernet, J. Schmiedmayer, and A. Zeilinger, *Phys. Rev. Lett.* **77**, 4980 (1996).
- ²¹ M. Hiller, T. Kottos, and A. Ossipov, *Phys. Rev. A* **73**, 063625 (2006).
- ²² E. M. Graefe, H. J. Korsch, and A. E. Niederle, *Phys. Rev. Lett.* **101**, 150408 (2008);
- ²³ K. F. Zhao, M. Schaden, and Z. Wu, *Phys. Rev. A* **81**, 042903 (2010).
- ²⁴ J. Schindler, A. Li, M. C. Zheng, F. M. Ellis, and T. Kottos, *Phys. Rev. A* **84**, 040101(R) (2011).
- ²⁵ J. Schindler, Z. Lin, J. M. Lee, H. Ramezani, F. M. Ellis, and T. Kottos, *J. Phys. A: Math. Theor.* **45**, 444029 (2012).
- ²⁶ N. Lazarides and G. P. Tsironis, *Phys. Rev. Lett.* **110**, 053901 (2013).
- ²⁷ C. Yuce, *Phys. Lett. A* **378**, 2024 (2014).
- ²⁸ Q.-B. Zeng, S. Chen, and R. Lü, *Phys. Rev. A* **95**, 062118 (2017).
- ²⁹ A. F. Tzortzakakis, K. G. Makris, and E. N. Economou, *Phys. Rev. B* **101**, 014202 (2020).
- ³⁰ I. Rotter and J. P. Bird, *Rep. Prog. Phys.* **78**, 114001 (2015).
- ³¹ L. -L. Zhang and W. -J. Gong, *Phys. Rev. A* **95**, 062123 (2017).
- ³² L. -L. Zhang, Z. -Z. Li, G. -H. Zhan, G. -Y. Yi, and W. -J. Gong, *Phys. Rev. A* **99**, 032119 (2019).
- ³³ P. C. Burke, J. Wiersig, and M. Haque, *Phys. Rev. A* **102**, 012212 (2020).
- ³⁴ P. W. Anderson, *Phys. Rev.* **109**, 1492 (1958).
- ³⁵ P. A. Lee and T. V. Ramakrishnan, *Rev. Mod. Phys.* **57**, 287 (1985) and references therein.
- ³⁶ N. Mott, *J. Phys. C* **20**, 3075 (1987).
- ³⁷ E. Abrahams, P. W. Anderson, D. C. Licciardello, and T. V. Ramakrishnan, *Phys. Rev. Lett.* **42**, 673 (1979).
- ³⁸ S. Aubry and G. Andre, *Ann. Israel Phys. Soc.* **3**, 133 (1980).
- ³⁹ P. G. Harper, *Proc. Phys. Soc. A* **68**, 874 (1955).
- ⁴⁰ M. Verbin, O. Zilberberg, Y.E. Kraus, Y. Lahini, and Y. Silberberg, *Phys. Rev. Lett.* **110**, 076403 (2013).
- ⁴¹ Y. E. Kraus, Y. Lahini, Z. Ringel, M. Verbin, and O. Zilberberg, *Phys. Rev. Lett.* **109**, 106402 (2012).
- ⁴² J. B. Sokoloff, *Phys. Rep.* **126**, 189 (1985).
- ⁴³ B. Simon, *Adv. Appl. Math.* **3**, 463 (1982).
- ⁴⁴ D. J. Thouless, *Phys. Rep.* **13**, 93 (1974).
- ⁴⁵ C. M. Soukoulis and E. N. Economou, *Phys. Rev. Lett.* **48**, 1043 (1982).
- ⁴⁶ F. J. Wegner, *Z. Phys. B* **36**, 209 (1980).
- ⁴⁷ J. Biddle and S. Das Sarma, *Phys. Rev. Lett.* **104**, 070601 (2010).
- ⁴⁸ S. Sil, S. K. Maiti, and A. Chakrabarti, *Phys. Rev. Lett.* **101**, 076803 (2008).
- ⁴⁹ H. P. Lüschen, S. Scherg, T. Kohlert, M. Schreiber, P. Bordia, X. Li, S. Das Sarma, and I. Bloch, *Phys. Rev. Lett.* **120**, 160404 (2018).
- ⁵⁰ D. Delande and G. Orso, *Phys. Rev. Lett.* **113**, 060601 (2014).
- ⁵¹ S. Y. Jitomirskaya, *Ann. Math.* **150**, 1159 (1999).
- ⁵² M. Rossignolo and L. Dell'Anna, *Phys. Rev. B* **99**, 054211 (2019).
- ⁵³ S. Roy and S. K. Maiti, *Eur. Phys. J. B* **92**, 267 (2019).
- ⁵⁴ S. Roy, S. K. Maiti, L. M. Peřez, J. H. O. Silva, and D. Laroze, *Materials* **15**, 597 (2022).
- ⁵⁵ M. Johansson, R. Riklund, *Phys. Rev. B* **42**, 8244 (1990).
- ⁵⁶ S. Ganeshan, K. San, and S. Das Sarma, *Phys. Rev. Lett.* **110**, 180403 (2013).
- ⁵⁷ S. Ganeshan, J.H. Pixley, and S. Das Sarma, *Phys. Rev. Lett.* **114**, 146601 (2015).
- ⁵⁸ S. Das Sarma, S. He, and X. C. Xie, *Phys. Rev. Lett.* **61**, 2144 (1988).
- ⁵⁹ S. Das Sarma, S. He, and X. C. Xie, *Phys. Rev. B* **41**, 5544 (1990).
- ⁶⁰ T. Liu and H. Guo, *Phys. Rev. B* **98**, 104201 (2018).
- ⁶¹ T. Liu and H. Guo, *Phys. Rev. B* **96**, 174207 (2017).
- ⁶² W. P. Su, J. R. Schrieffer, and A. J. Heeger, *Phys. Rev. Lett.* **42**, 1698 (1979).
- ⁶³ M. Yahyavi, B. Hetényi, and B. Tanatar, *Phys. Rev. B* **100**, 064202 (2019).
- ⁶⁴ A. Eilmes, R. A. Römer, and M. Schreiber, *Eur. Phys. J. B* **23**, 229 (2001).
- ⁶⁵ E. J. Meier, F. Alex An, and B. Gadway, *Nat. Commun.* **7** 13986(2016).
- ⁶⁶ S. Roy, T. Mishra, B. Tanatar, and S. Basu, *Phys. Rev. Lett.* **126**, 106803 (2021).
- ⁶⁷ S. Bid and A. Chakrabarti, *Phys. Lett. A* **423**, 127816 (2022).
- ⁶⁸ Y. Aharonov and D. Bohm, *Phys. Rev.* **115**, 485 (1959).
- ⁶⁹ H. F. Cheung, Y. Gefen, E. K. Reidel, and W. H. Shih, *Phys. Rev. B* **37**, 6050 (1988).
- ⁷⁰ M. Büttiker, Y. Imry, and R. Landauer, *Phys. Lett. A* **96**, 365 (1983).
- ⁷¹ L. P. Levy, G. Dolan, J. Dunsmuir, and H. Bouchiat, *Phys. Rev. Lett.* **64**, 2074 (1990).
- ⁷² V. Chandrasekhar, R. A. Webb, M. J. Brady, M. B. Ketchen, W. J. Gallagher, and A. Kleinsasser, *Phys. Rev. Lett.* **67**, 3578 (1991).
- ⁷³ E. M. Q. Jariwala, P. Mohanty, M. B. Ketchen, and R. A. Webb, *Phys. Rev. Lett.* **86**, 1594 (2001).
- ⁷⁴ S. -D. Liang, Z. D. Wang, and J. -X. Zhu, *Solid State Commun.* **98**, 909 (1996).
- ⁷⁵ H. Bouchiat and G. Montambaux, *J. Phys. (Paris)* **60**, 2695 (1989).
- ⁷⁶ R. A. Smith and V. Ambegaokar, *Europhys. Lett.* **20**, 161 (1992).
- ⁷⁷ H. Chen, E. Zhang, K. Zhang, S. Zhang, *RSC Adv.* **5**, 45551 (2015).
- ⁷⁸ S. K. Maiti, M. Dey, S. Sil, A. Chakrabarti, and S. N. Karmakar, *Europhys. Lett.* **95**, 57008 (2011).
- ⁷⁹ H. F. Cheung and E. K. Riedel, *Phys. Rev. Lett.* **62**, 587 (1989).
- ⁸⁰ H. Bluhm, N. C. Koshnick, J. A. Bert, M. E. Huber, and K. A. Moler, *Phys. Rev. Lett.* **102**, 136802 (2009).
- ⁸¹ P. A. Orellana and M. Pacheco, *Phys. Rev. B* **71**, 235330 (2005).
- ⁸² V. Ambegaokar and U. Eckern, *Phys. Rev. Lett.* **65**, 381 (1990).
- ⁸³ N. O. Birge, *Science* **326**, 244 (2009).
- ⁸⁴ S. K. Maiti, J. Chowdhury, and S. N. Karmakar, *Phys. Lett. A* **332**, 497 (2004).
- ⁸⁵ S. K. Maiti, J. Chowdhury, and S. N. Karmakar, *J. Phys.: Condens. Matter* **18**, 5349 (2006).
- ⁸⁶ J. Majhi and S. K. Maiti, *J. Phys.: Condens. Matter* **12**, 12 (2020).
- ⁸⁷ A. Koley and S. K. Maiti, *Eur. Phys. J. Plus* **137**, 15 (2022).

- ⁸⁸ D. Xie, W. Gou, T. Xiao, B. Gadway, and B. Yan, *Npj Quantum Inf.* **5**, 55 (2019).
- ⁸⁹ X. L. Lü and H. Xie, *J. Phys.: Condens. Matter* **31** 495401 (2019).
- ⁹⁰ L. Jin, P. Wang, and Z. Song, *Sci. Rep.* **7**, 5903 (2017).
- ⁹¹ Y. Zhang, B. Ren, Y. Li, and F. Ye, *Opt. Express* **29**, 42827 (2021).
- ⁹² Z. G. Chen, L. Wang, G. Zhang, and G. Ma, *Phys. Rev. Applied* **14**, 024023 (2020).
- ⁹³ H. Kato and D. Yoshioka, *Phys. Rev. B* **50**, 4943 (1994).
- ⁹⁴ T. Liu and H. Guo, *Phys. Lett. A* **382**, 45 (2018).
- ⁹⁵ B. S. Shastry and B. Sutherland, *Phys. Rev. Lett.* **65**, 243 (1990).
- ⁹⁶ A. Kambili, C. J. Lambert, and J. H. Jefferson, *Phys. Rev. B* **60**, 7684 (1999).
- ⁹⁷ S. Gupta, S. Sil, and B. Bhattacharyya, *Physica B* **355**, 299 (2005).
- ⁹⁸ R. Deblock, R. Bel, B. Reulet, H. Bouchiat, and D. Mailly, *Phys. Rev. Lett.* **89**, 206803 (2002).
- ⁹⁹ L. Thatcher *et al.*, *Phys. Scr.* **97**, 035702 (2022).
- ¹⁰⁰ E. J. Meier, F. A. An, and B. Gadway, *Nat. Commun.* **7**, 13986(2016).
- ¹⁰¹ S. Roy, S. Ganguly, and S. K. Maiti, *Sci. Rep.* **13**, 4093 (2023).
- ¹⁰² S. Roy and S. K. Maiti, *J. Phys.: Condens. Matter* **35**, 355303(2023).